The 8th International Supercritical CO_2 Power Cycles Symposium
February 27 – 29, 2024, San Antonio, Texas
Paper #63

High-Temperature Creep and Creep-Fatigue Performance of Stainless Steel 316 Diffusion Bonds

John Shingledecker, Ph.D., FASM
Electric Power Research Institute
Charlotte, NC USA

Dr. Shingledecker, is a Principal Technical Executive in EPRI's Energy Supply & Low-Carbon Resources research area with responsibility for Technology Innovation, strategic planning, and technical leadership of collaborative projects focused on advanced manufacturing methods and materials. His 20+ years of research in the high-temperature behavior of engineering materials includes over 200 publications and multiple awards for technology transfer to industry.

Vikash Kumar
Electric Power Research Institute (EPRI)
Charlotte, NC USA
Mr. Kumar is an engineer conducting research in EPRI's Welding & Repair Technology Center where he has been since 2002 after graduating from North Carolina State University with a B.S. in Materials Science and Engineering.

Andrea Bollinger, Ph.D.
Electric Power Research Institute (EPRI)
Charlotte, NC USA
Dr. Bollinger earned a Metallurgy and Materials Engineering PhD from Colorado School of Mines in 2020. Since then, she has conducted metallurgy research during a post-doctorate appointment at Carnegie Mellon University within the Center for Iron and Steelmaking and EPRI's Materials & Repair Program.

Bonnie Antoun, Ph.D.
Sandia National Laboratories
Livermore, CA USA
Dr. Antoun is a Distinguished Member of Technical Staff and leads the Experimental Mechanics laboratory at Sandia National Laboratories in Livermore, CA. Her research projects range from discovery to characterization of complex engineering materials, to developing validation data sets for thermomechanical behavior of engineering systems in extreme environments.

Dereje Amogne, Ph.D.
VPE Thermal, LLC
Sacramento, CA USA
Dr. Amogne is the General Manager at VPE Thermal LLC and chief design engineer for various heat exchangers and processes. He has PhD in thermal engineering and has over 20 years of experience in designing compact heat exchangers for extreme process conditions and introduced various novel ideas to improve heat exchanger performance and reduce cost.

Kevin Albrecht, Ph.D.
VPE Thermal, LLC
Sacramento, CA USA
Dr. Albrecht is a Senior Engineer at VPE Thermal LLC and primarily works on novel heat exchanger design and manufacturing for R&D projects. Prior to VPE, he worked at Sandia National Laboratories where he led projects on heat exchanger development for the application of solar thermal driven supercritical CO_2 power cycles. Dr. Albrecht has over 10 years of experience developing models and conducting experiments for engineering R&D projects.

Matthew Sandlin, Ph.D.
Sandia National Laboratories
Albuquerque, New Mexico
Dr. Sandlin has nearly a decade of experience in CSP R&D in both academic and industrial settings. He is the responsible engineer for the primary heat exchanger in Sandia National Lab's G3P3 project, and experience in testing and characterization of advanced heat exchanger prototypes.

ABSTRACT

In support of an effort to develop a model for determining the lifetime of a diffusion bonded supercritical CO_2 (sCO_2) recuperators and solid particle to sCO_2 compact heat exchangers (CHX) in concentrated solar power applications, a commercially produced stainless steel alloy 316L diffusion bonded block was characterized. An extensive test program involving high-temperature tensile, creep, low-cycle fatigue (LCF) and low-cycle fatigue with hold times (creep-fatigue) was conducted at temperatures up to 700°C to enable applications up to the current code allowable application temperature of 649°C. High-temperature tensile strength was found to be at the minimum of the wrought scatter band. Conversely, analysis of the creep and fatigue data showed the diffusion bonded block performance was within the wrought scatter band of 316 and 316H. A modest reduction in cycle life was found with imposition of a tensile hold in the fatigue cycle which was less than predicted by current ASME 'creep-fatigue' interaction diagram. Post-test evaluations of tested samples show inhomogeneous distributions of damage and strain with samples failing near bond lines in an oval shape. Limited creep tests on the starting sheets confirmed non-isotropic high-temperature strength to be the source of the ovality. Microstructural analysis suggest grain boundary features near bonds lines may contribute to preferential damage initiation. Overall, the mechanical results showed good ductility and strength levels equivalent to 316/316H, so current lifetime design approaches based on ASME Section III Division 5 could be utilized for component design. Component feature tests and cyclic operation of a test article is proposed to validate and improve component lifetime predictions for diffusion bonded heat exchangers and recuperators.

INTRODUCTION

Diffusion bonded (DB) compact heat exchangers (HX) are candidate components in both direct and indirect supercritical CO_2 (sCO_2) power cycle applications. Their highly efficient performance, needed for recuperation and heat-exchange, can reduce the plant footprint and capital costs compared to more traditional HXs [1,2]. For Generation 3 (Gen 3) concentrating solar power (CSP) applications using solid particles as the heat-transfer media, a falling particle to sCO_2 DB-CHX has been designed in the U.S. DOE Gen 3 Particle Power Plant (G3P3) on-sun demonstration of a falling particle CSP system including thermal energy storage and power generation [3, 4]. To achieve high overall cycle efficiency for CSP and sCO_2 power generation system, higher temperatures are desired. Due to the high-temperature and cyclic loading anticipated for daily cycling of a future CSP powerplant, time dependent and cyclic damage mechanisms including creep, low cycle fatigue (LCF) and possible creep-fatigue interactions are considered for HX design.

DB-HXs are designed to ASME Boiler & Pressure Vessel (B&PV) Code Section VIII which does not specify a design life. Furthermore, the effect of the DB manufacturing on high-temperature performance is not well characterized. Most studies of high-temperature creep on stainless steel 316, iron-nickel alloy 800H, and nickel-based alloy 617 have shown diffusion bonds to have inferior creep strength compared to expected wrought performance [5-8]. However, some of these studies were performed on laboratory single bonds which may not be representative of commercial practice. A recent study of creep performance on a commercially produced diffusion bond of alloy 316 found that rupture lives in long-term creep tests to times from ~100 to ~8,000 hours were within the scatter band for wrought 316 [9]. The study also found that for some test conditions small samples produced longer lifetimes than typical sample sizes and proposed that post-test observations of sample ovality was due to anisotropy in the starting sheet stock used in the diffusion bonding process. Additionally, short-term creep damage was concentrated on

the diffusion bond line although macroscopic creep ductility was high. Therefore, this study was conducted to provide critical data to improve the lifetime models and understand the damage process under creep, fatigue, and potential creep-fatigue interaction for DB-HX made of stainless steels to provide end-user confidence in the technology.

MATERIAL & EXPERIMENTAL PROCEDURES

An ~200mm x ~200mm x ~133mm thick (8 x 8 x 5.25 inch) commercially diffusion bonded block made from 1.5mm thick (16 gauge) 316L stainless steel sheets with the composition shown in Table 1 was used for this study. Starting sheet stock subjected to the same diffusion bonding thermal profile (no applied stress) was also evaluated. The bonding process and material conformed to ASME BPVC Code Section IX QW185 and Code Case 2577 (ensures grain size <ASTM 7 to allow use up to 649°C), respectively [10, 11].

Table 1. *Composition of the 316L stainless steel sheet (vendor) and DB block (EPRI measured) compared to the specification minimums (min) and maximums (max) for 316L (wt. %)*

316L	**C**	**Si**	**Mn**	**P**	**S**	**Ni**	**Cr**	**Nb**	**Cu**	**N**	**B**	**Co**	**Mo**	**Ti**
Min						*10.0*	*16.0*						*2.00*	
Max	*0.030*	*0.75*	*2.00*	*0.045*	*0.030*	*14.0*	*18.0*			*0.10*			*3.00*	
Vendor	0.021	0.48	0.91	0.036	0.001	10.1	17.1			0.040			2.03	
EPRI	0.022	0.548	0.94	0.035	<0.0005	10.07	17.233	0.037	0.411	0.0412	<0.002	0.24	2.04	<0.002
	V	**W**	**As**	**Sb**	**Sn**	**O**	**Ca**	**Fe**	**Al**	**La**	**Ta**	**Zr**	**Bi**	**Pb**
EPRI	0.076	<0.005	0.007	0.001	N/A	0.0024	<0.002	68.28	0.006	<0.002	<0.005	<0.002	<0.0001	0.00004

Samples for tensile, creep, low cycle fatigue (LCF) and LCF + hold-time testing were extracted through the block thickness, so diffusion bonds were tested perpendicular to the applied stress. Tensile and creep tests were conducted on sample with a 12.7mm diameter at temperatures up to 750°C. Strain controlled LCF and LCF+hold-time tests were conducted on samples with a 6.35mm diameter near the intended operational temperature of 600°C with a strain rate of 0.001/sec, a R-ratio of -1 (fully reversed), and strain ranges of 0.7 to 1.5%. For hold-time tests, 30 minute tensile holds were employed. Creep testing of sheet samples used pin-loaded grips in dead-load creep frames in the same manner as described in ref [12].

Prior to sectioning, fracture surfaces were analyzed using a Keyence VR-3200 LED optical microscope, and eccentricity (e) measurement to quantify ovality were made by measuring the minor and major axis (A, B) per the equation:

$$e = \sqrt{1 - \frac{(0.5 * B)^2}{(0.5 * A)^2}}$$

Samples were prepared for post-test cross-sectional metallurgical analysis by sectioning along the longitudinal axis using wire electrical discharge machining (EDM). They were mounted and polished using standard metallurgical techniques with selected samples having a final vibratory

polish of 0.02 µm. Optical metallography was conducted on all samples to using a VHX-7000 Optical Microscope and selected samples were further evaluated on an FEI Teneo Scanning Electron Microscope (SEM). EBSD maps were captured using a Hikar Pro high-speed electron backscatter diffraction (EBSD) detector and analyzed with EDAX Teams analysis software.

RESULTS

Duplicate tensile tests conducted at room temperature and 550 to 750°C all showed excellent repeatability with elongations greater than 50% (Figure 1a). The room temperature yield strength (YS) and ultimate tensile strength (UTS) exceeded the 316L minimum specification requirement. As shown in Figure 1b, the elevated YS and UTS were slightly below the ASME B&PV Code design yield (y1) and tensile strength (U) values for 316 and 316L. It should be noted that the ASME U and y1 values are not minimum requirements nor a statistical minimum design curve; they are developed based on an average trend curve which is adjusted to the specification room temperature tensile minimums.

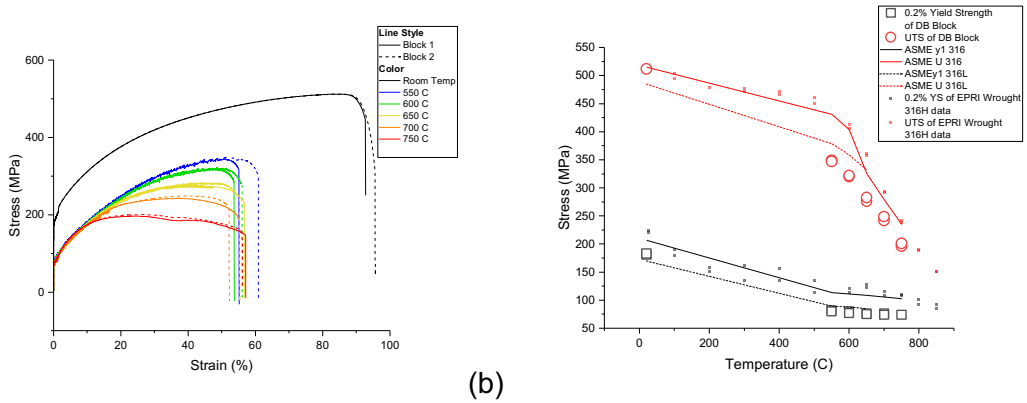

(a) (b)

Figure 1. *Tensile test stress-strain curves (a) and yield strength (YS) and ultimate tensile strength (UTS) compared to ASME y1 and U curves (b) for 316 DB*

Creep-rupture tests were conducted at 600, 650, and 700°C on diffusion bonds for times exceeding 10,000 hours as shown in Figure 2. Rupture elongation (for completed tests) was greater than 20% and all curves showed appreciable time in the tertiary creep regime. For comparison, creep tests were performed on the starting sheet after being heat-treated with the same thermal profile (no pressure loading) as the DB block. The sheets were tested in two orientations, and the results show the sheets tested parallel to the rolling direction had the lowest creep rates and longest rupture lives (Figure 3), and that irrespective of orientation, the sheets exhibited lower creep rates than the DB block.

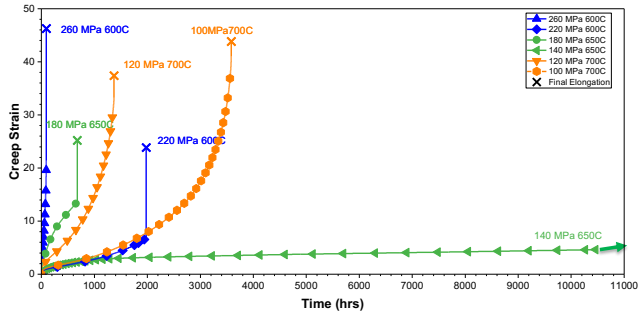

Figure 2. *Creep strain versus time curves for DB creep tests, arrow indicates ongoing test*

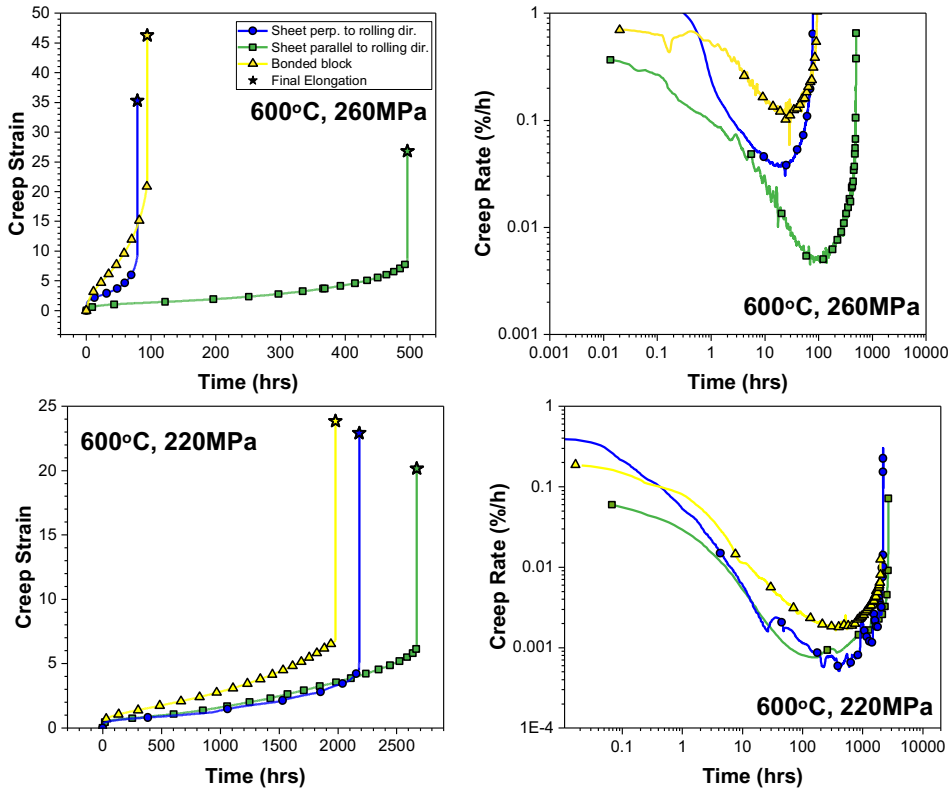

Figure 3. *Creep strain and creep rate versus time curves for diffusion bonds compared to individual sheets given an equivalent heat-treatment to the bonding conditions and tested in multiple orientations.*

Six LCF tests were conducted at 600°C and strain ranges from 0.07 to 0.015 with resulting cycles to failure from a few hundred cycles to >4,000 cycles (Figure 4). The data appear well in-line with wrought 316H expectations based on data from Ref. [13]. Three longer-term LCF+hold-time tests using a 30 minute hold-time, which is suggested in wrought 316 to introduce a 'creep-fatigue' interaction [14], was found to reduce the cyclic life by a factor of ~2 in a strain range of 0.013 to 0.015 (X datapoints in Figure 4).

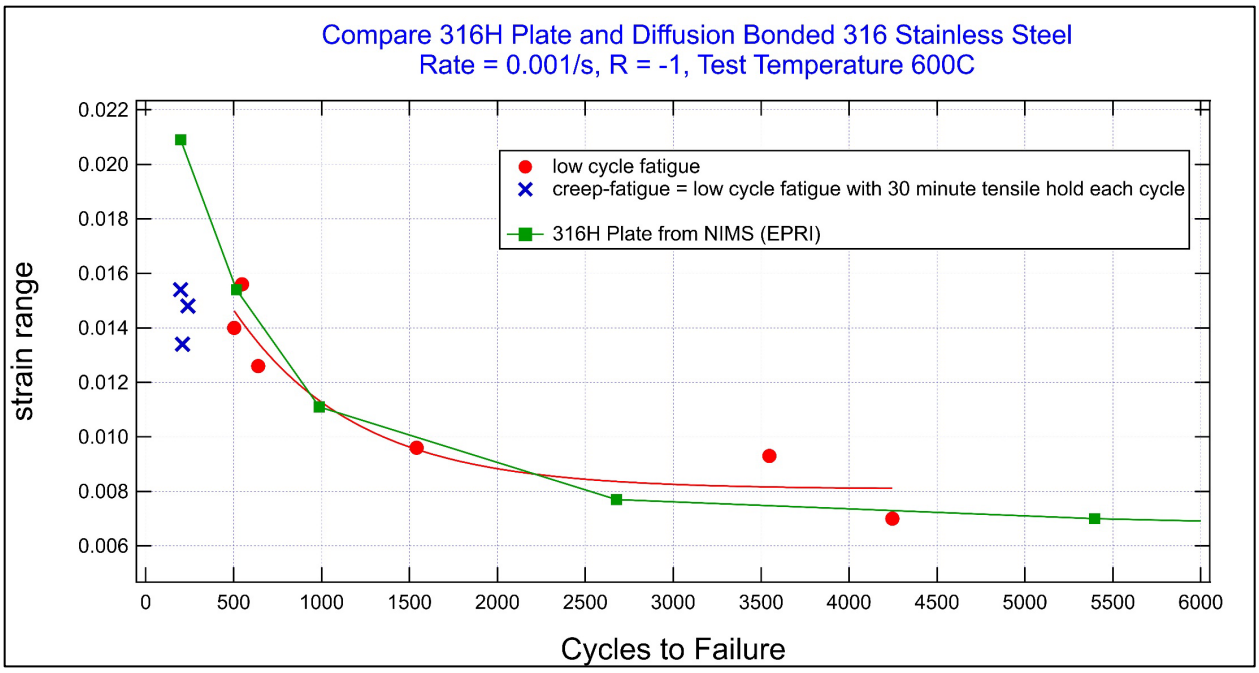

Figure 4. *Cycle to failure (S-N) curve developed for 316 DB compared to expected wrought performance and LCF+hold-time tests*

Post-test inspection of the creep samples showed most samples had an oval cross-section with eccentricity values ranging from 0.42 to 0.67 (Table 2). Creep ductility (elongation and reduction of area) was higher in samples with higher levels of eccentricity. The creep samples had non uniform cross-sections (Figure 5) with multiple regions of undulating deformation (minor necking) and measurable elongation between diffusion bond layers throughout the sample gauge. Creep damage (Figure 6), cracking, and failure was observed in the diffusion bonded regions in all samples resulting in a flat 'brittle-like' macroscopic appearance although the sample had undergone significant deformation prior to failure. At 600 and 650°C, the damage was predominately observed in the diffusion bonded areas, but at 700°C near the failure, creep damage (cavities) was also observed in the regions between the diffusion bonds as indicated in Figure 6. Some evidence of surface cracking was also found in the 700°C samples similar to prior work [9].

Table 2*. Post-creep test ovality measurement*

Stress (MPa)	Temperature (°C)	Rupture Life	Elongation	Reduction of Area	Eccentricity (eqn. 1)
260	600	93.8	46.3	51.4	0.67
220	600	1978.9	23.8	22.3	0.49
180	650	678.8	25.2	24.5	0.42
140	650	10469*	4.6*	-	-
120	700	1371.1	37.4	39.3	0.59
100	700	3585.1	43.8	56.0	0.66

**In-test*

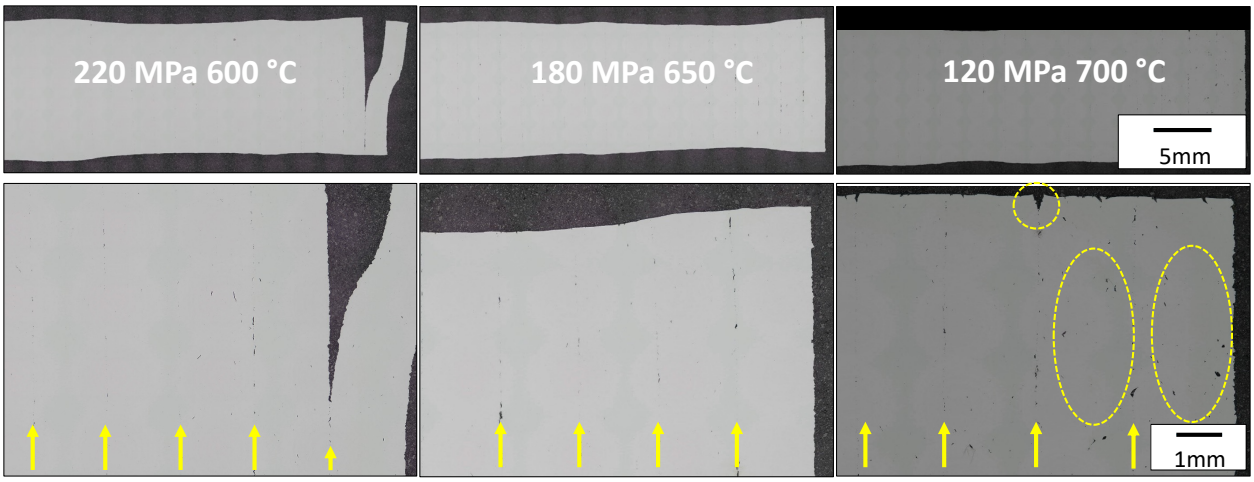

Figure 5. *Post-test optical micrographs (unetched) showing morphology of creep damage. Yellow arrows indicate location of diffusion bonds, dashed circle indicated surface cracking and the large dashed ovals highlight creep damage away from diffusion bonds.*

Optical evaluation of the LCF and LCF+hold-time tests at 600°C showed multiple surface cracks. Metallographic cross-sections (Figure 6) showed the LCF tests to have a large population of surface cracks which occurred both at surface-bond-line interfaces and in the bulk material. Fracture appearance was flat and macroscopically 'brittle-like' with failures at a bond line region, but, similar to the creep samples, deformation was observed along the gauge length. In one case, the ductility of the sample was evident as multiple cracks extending through half the sample diameter were observed (Figure 6 – right).

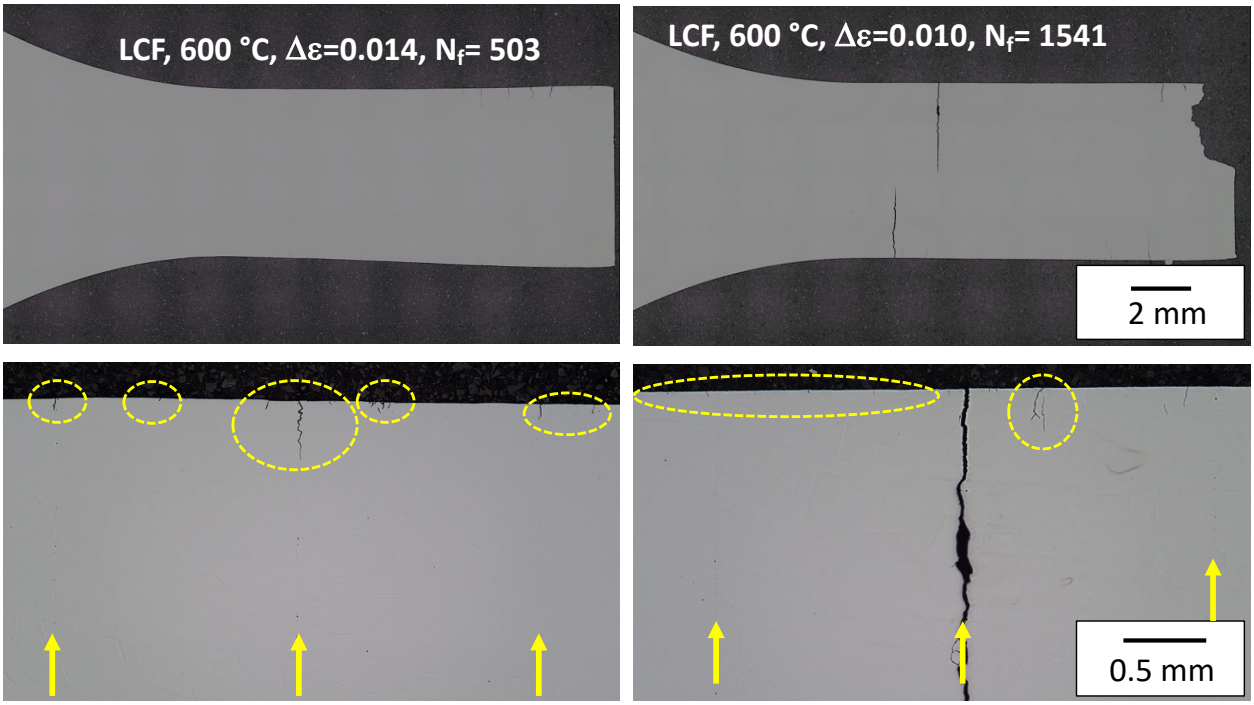

Figure 6. *Post-test optical micrographs (unetched) showing morphology of damage after LCF tests. Arrows indicate location of diffusion bonds, dashed circles highlight locations of surface-initiated cracking.* $\Delta\varepsilon$ *= strain range,* N_f *= number of cycles to failure*

Initial characterization (Figure 7) of the starting sheet, prior to diffusion bonding, showed a fine grain size with an average size of 12.4 μm which is equivalent to ASTM grain size of 9. After the diffusion bonding cycle, the average grain size was measured to be 155 μm which is equivalent to ASTM grain size of 2. This grain size meets the requirement of Code Case 2557 [11] which requires the 316L to have a grain size coarser than ASTM 7 and allows the 316L to utilize 316 stress allowables to 649°C.

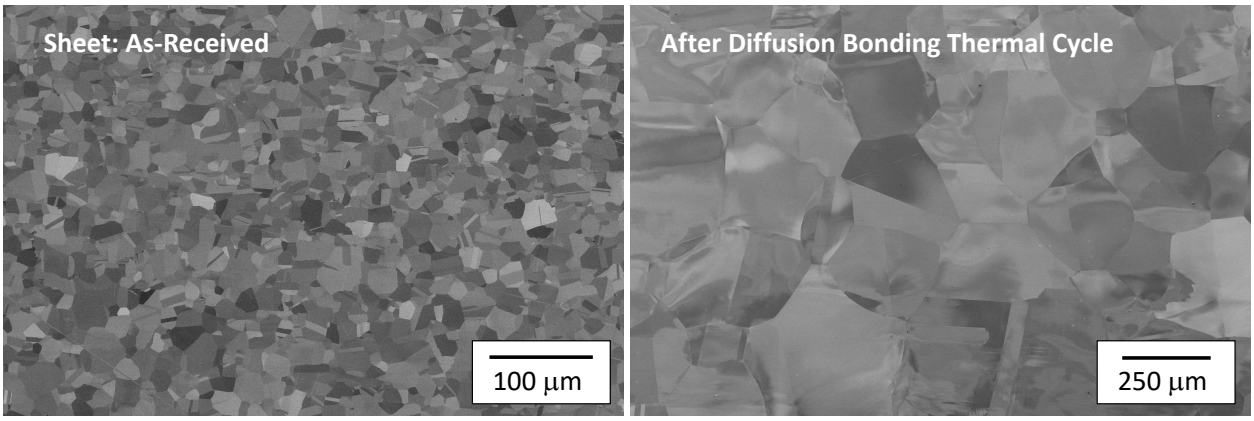

***Figure 7**. SEM comparison of grain size prior to bonding (starting sheet) and after bonding*

DISCUSSION

The tensile test data (Figure 1) confirmed the bonded block met the 316L specification requirements and all the tests showed a high degree of repeatability in terms of strength and ductility suggesting that the bonding process was well controlled and there were no significant bond interface issues (delamination, contamination, etc.). The elevated temperature YS and UTS were slightly below the ASME y1 and U tabular values for 316L and as expected below higher strength 316/316H values. Inspection of the tensile curves show that for all tests the samples reached an UTS prior to necking and failure, so poor bonding or poor overall ductility is not causing the lower tensile strength. C, N, Mo, and Si all have a solid solution strengthening effect in stainless steels [15] and this heat of 316L has typical C, N, and Si levels with Mo at the specification minimum which may have some influence on the YS and UTS. Grain size also has a direct impact on tensile properties in 316 stainless steel with larger grain sizes causing increased tensile ductility but decreased tensile strength [16, 17]. As previously noted, a measured YS or UTS below the ASME U and y1 tensile curves does not indicate a material acceptance or design issue as these curves are not statistical minimums but rather assume a distribution of performance.

To explore the creep performance of the DB, the time-to-rupture data were compared to EPRI's 316/316H database. The 316/316H database was used for comparison because this heat of 316L also met the chemistry requirements for 316 and after diffusion bonding had a coarser grain size which allows the use of 316 stress allowables. Additionally, there is considerable scatter and overlap between the 316L, 316, and 316H available creep data with complexities associated with unspecified elements which influence creep behavior such as N, which has shown to be more important in enhancing creep strength than C [18], and, for this heat of 316L, was measured at 0.04 wt.% which is greater than the amount of C at 0.03 wt.%. Figure 8 compares the rupture lives and ongoing tests on the diffusion bonded block and sheets to this database by use of the Larson Miller Parameter (LMP) with a constant of C = 20. Inspection of

the data show the DB block and sheets all have rupture lives within the 316/316H scatter band. Additionally, standard sample size data on a commercial 316 DB from ref [9] is also plotted which overlaps this work. This suggests that the chemistry of this heat (which was also the heat used in ref [9]) combined with coarser grain sizes results in a 'L-grade' stainless steel having creep strength of a 'H-grade' material. Closer inspection of the data show that at the highest stress, the data on the DB trends towards the bottom of the scatter band while lower stress tests trend towards the upper end of the scatter band. This transition is likely due to how creep deformation and fracture mechanisms are manifest in a coarser grain material. As previously discussed, coarser grains have reduced tensile strength at high temperature which is controlled by the flow of dislocation through the bulk material which is similar to the mechanisms of creep deformation at higher stress. However, as stress is decreased (and temperature is increased) in alloy 316, creep deformation is controlled by the diffusional processes near grain boundaries [19] and so for coarser grained materials, which have less grain boundaries per unit area, the creep strength is increased which is what is observed for these tests. The measured ovality of the creep samples (Table 2) was previously postulated [9] to be the result of the starting sheet having anisotropic creep behavior which was confirmed by multiple tests (Figure 3). At the higher stress tests, the creep life was over 6X longer and the minimum creep rate was lower by an order of magnitude for sample testing parallel to the rolling direction when compared with the sample perpendicular to the rolling direction. As stress was decreased minimal differences were observed. The corresponding DB performance showed notable trends. The DB rupture life was similar to the weaker of the two sheet orientations, but the creep rates were significantly higher in the DB compared to the sheet even for similar rupture lives. The metallurgical evidence for preferential creep damage initiation in the diffusion bond areas (Figure 5) may be evidence of potential early damage initiation leading to creep acceleration compared to the bulk sheet behavior. However, if this small damage region is constrained by the surrounding sheet, then the rupture life is still largely controlled by the bulk behavior.

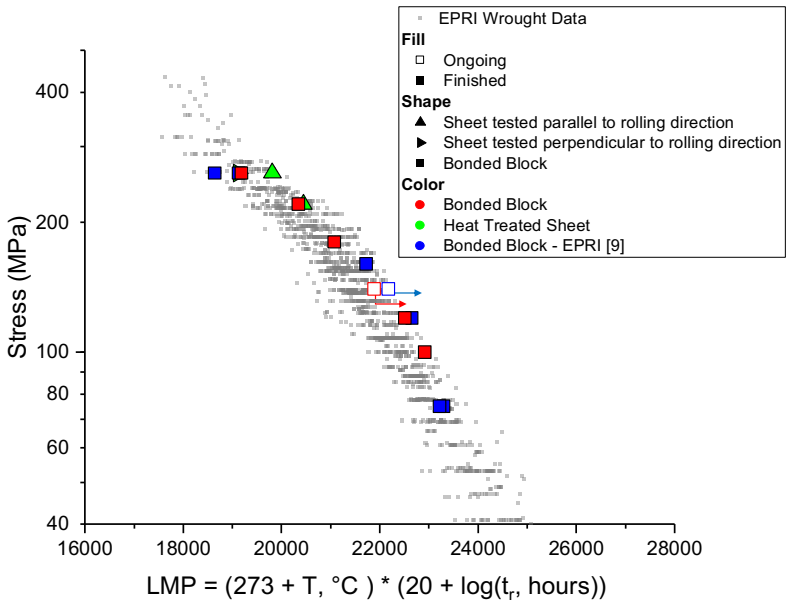

Figure 8. *Larson Miller Parameter (LMP) plot comparing the creep time to rupture results for the DB block and sheets in this study with prior work by EPRI on a 316 commercially produced diffusion bonded block [9] and EPRI's database for creep of 316/316H.*

The LCF cycle life for the DB and fit cycles-to-failure (S-N) curve plotted in Figure 4 is essentially equivalent to literature data and expectations. No significant deviations were observed for LCF life. The 30 minute hold-time only reduced cycle life by a factor of 2 which is consistent with literature data in the range of 600 to 650°C [14]. While additional analysis is required to calculate the 'creep-fatigue' damage interaction, the lack of a significant interaction indicates traditional design approaches based on ASME B&PV Code Section III Division 5 and modifications suggest existing allowable stress values for 316 can be used for simplified fatigue and creep-fatigue analysis for CSP components [20].

The post-test failure morphology appeared to have similarities and difference based on optical analysis (Figures 5 and 6). Both samples showed macroscopic ductility but flat fracture faces indicating ultimate failure was associated with the original diffusion bond interface. In the case of creep, the samples appeared to show a majority of cavities and cracking along diffusion bond regions while the fatigue samples showed many small surface-initiated cracks with some growing deeper into the sample cross-section at number and occurrence much greater than the number of diffusion bonds. SEM analysis, Figure 9, evaluates damage at diffusion bonds near the failure which showed damage. As seen in Figure 9a, a LCF crack is observed growing transgranular but linking between pre-existing voids from the original diffusion bond interface. Conversely, in Figure 9b, intergranular creep damage is observed along grain boundaries which have clearly migrated (grown) during the diffusion bonding process and are not directly intersecting the pre-existing voids. Prior research on 316 diffusion bonded blocks showed qualified bonds which exhibit clear evidence of 'good bonding,' as evidenced by grain growth across the diffusion bond interface and pass the optical metallography requirements for ASME Section IX, can still have a small number of isolated voids <5μm in size, and these voids can be inter or intragranular [9].

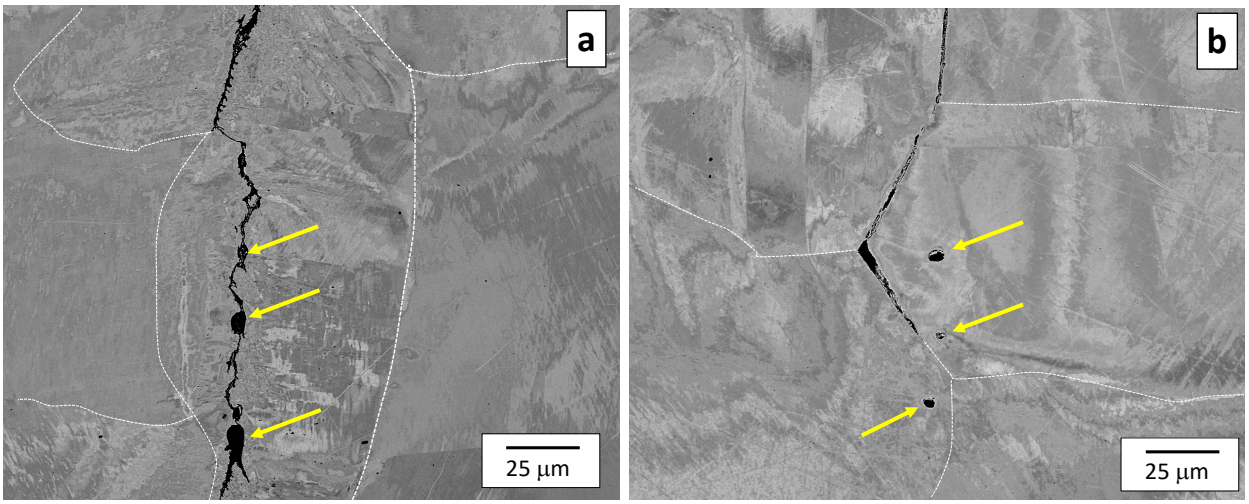

Figure 9 . *Transgranular fatigue crack (a) and intergranular creep crack (b) taken on diffusion bond lines showing significant damage but not failure. Applied stress is horizontal to images. White dashed lines indicate location of grain boundaries, and yellow arrows indicate pre-existing voids along original diffusion bond interface.*

Due to the large strains accommodated in the microstructure during the failure process, it can be difficult to interpret some of the SEM images. Therefore, to study the creep damage initiation process, a diffusion bond line 7 bonds removed from the failure (significantly away from the failure) where strains are lower and advanced creep damage was not observed (no microcracks) was examined. The pre-existing voids are seen along the original diffusion bond interface with

grain boundaries which have clearly migrated beyond the original interface (Figure 10a) as described previously. EBSD was used to create Kernal Average Misorientation (KAM) maps which indicate localization of strain within the microstructure. As shown in Figure 10b, the brighter regions indicate higher strains generally along grain boundaries which can be indicative of a precursor to grain boundary damage [20]. As found previously in the optical images, the creep damage was concentrated normal to the applied stress. Careful inspection of Figure 10b shows that the grain boundaries normal to the applied stress near the diffusion bond line show the most damage while grain boundaries one grain removed from the diffusion bond region had little to no measurable orientation change (indicative of low internal strain). The regions surrounding the pre-existing voids are also elevated in strain. Thus, for creep it appears that damage is not initiating on the bond line or on the small pre-existing voids, but rather the pre-existing voids are acting as local stress concentration features leading to higher stresses on the grain boundaries in regions close to the void. However, additional characterization of multiple samples (test conditions) and regions is needed to substantiate this theory. As damage progresses, creep cavitation and microcracking initiates (See Figure 9b) on the grain boundaries in close proximity to the voids which lead to a macroscopic creep crack which is relatively flat in appearance (Figure 5). In contrast for LCF, crack initiation is at sample surfaces irrespective of location (near or away from diffusion bonds) and growth is transgranular. Cracks which initiate near diffusion bond interfaces are surmised to grow faster / preferentially because they can link between pre-existing voids (Figure 9a). This is seen most clearly at lower strain ranges (Figure 6b) where multiple large cracks extend over halfway through the sample at the diffusion bonds while many surface-initiated cracks away from diffusion bonds are arrested.

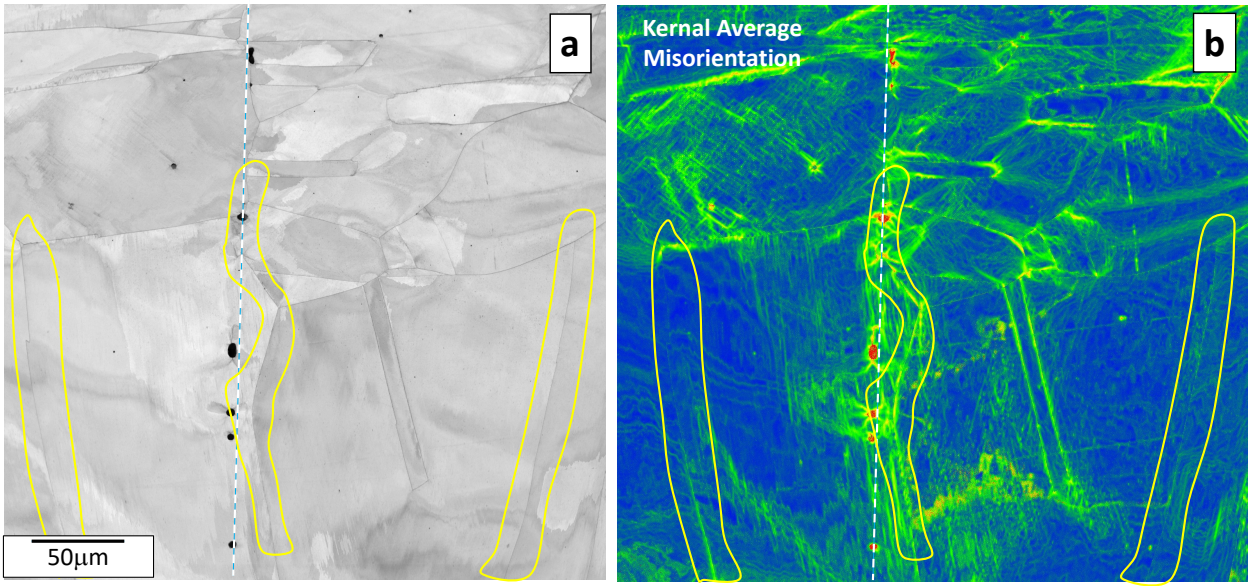

Figure 10. *SEM image (a) from the 7th diffusion bond line (dashed white line) removed from the creep failure location showing pre-existing diffusion bond line voids and three grain boundaries highlighted (yellow) normal to the applied stress (horizontal direction). SEM EBSD (b) shows higher levels of strain accumulating along grain boundaries near pre-existing voids compared to grain boundaries in similar orientations away from voids.*

CONCLUSIONS & FUTURE RESEARCH

An extensive study of a 316L commercially produced diffusion bonded stack in support of developing lifetime models for sCO_2 heat exchangers operating at high-temperatures was

conducted. Long-term creep tests exceeding 10,000 hours at 600 to 700°C, tensile tests up 750°C, and LCF and LCF+hold-time ('creep-fatigue') tests at the intended application temperature of 600°C all showed the diffusion bond met the wrought expectations with the creep, fatigue, and creep-fatigue performance achieving mechanical properties within the typical scatterbands for 316/316H performance. This is likely due to the large grain size from the diffusion bonding process and nitrogen content of the starting sheet. While samples generally failed in the area of the diffusion bonds, extensive ductility was observed with macroscopic deformation and reasonable ductility measurements. Based on these data, diffusion bonded heat-exchanger lifetime model development for 316L is recommended to use existing design rules for alloy 316 to 649°C without additional factors for weld joint efficiency or strength reductions.

Interesting observations in the detailed characterization of selected samples after testing suggest further study is needed to understand the likely damage progression and failure in actual diffusion bonded heat-exchangers. Testing of starting sheets subjected to the same thermal bonding conditions confirmed that ovality in creep-rupture samples was due to starting material anisotropy, and, while rupture life was nearly identical in the poorer performing orientation of the sheet, diffusion bonded samples showed higher creep rates. The microstructural analysis suggests that small pre-existing voids from the diffusion bonding process may act as stress concentration features which promote a small acceleration in creep damage in grain boundaries near the diffusion bond interface. This effect is subtle and appears to have a negligible effect on rupture life but an important effect on damage progression because the damage initiation is limited to a small plane, so the bulk sheet material constrains the damage. Conversely, in fatigue, these voids do not impact fatigue initiation, which is surface dominated, but these sites serve as fatigue growth paths leading to flat fracture faces. All of the testing conducted in this research was on a diffusion bonded stack of sheets in isothermal conditions. In reality for a diffusion bonded HX, the primary loading conditions will be multiaxial from internal pressure in channels, and the entire block will be subject to thermal cycling which will introduce further complexities for fatigue loading. Future work will involve the testing of 'feature tests' exploring the creep behavior using internally pressurized creep tests with prototypical channels to understand if the damage progression will be similar to these uniaxial experiments. Furthermore, thermal cycling experiments in a sCO_2 test loop are being designed to understand how thermal transients will influence fatigue loading. These experiments will be used to partially validate structural models for component lifetime which is using the baseline data from this study.

REFERENCES

[1] G.O. Musgrove. "Heat Exchangers for Supercritical CO2 Power Cycle Applications." Tutorial, 6th Int. sCO2 Power Cycle Symposium. March 27-29, 2018, Pittsburgh, PA. Available: http://sco2symposium.com/papers2018/tutorials/Musgrove_HeatExchangerTutorial.pdf

[2] Martin T. White, Giuseppe Bianchi, Lei Chai, Savvas A. Tassou, Abdulnaser I. Sayma, "Review of supercritical CO2 technologies and systems for power generation," Applied Thermal Engineering, Volume 185, 2021, 116447, ISSN 1359-4311, https://doi.org/10.1016/j.applthermaleng.2020.116447.

[3] Kevin J. Albrecht, Clifford K. Ho, "Design and operating considerations for a shell-and-plate, moving packed-bed, particle-to-sCO2 heat exchanger," *Solar Energy*, Volume 178, 2019, Pages 331-340, ISSN 0038-092X, https://doi.org/10.1016/j.solener.2018.11.065

[4] Clifford Ho et. al. "Gen 3 Particle Pilot Plant (G3P3) High-Temperature Particle System for

Concentrating Solare Power (Phase 1 and 2). SANDIA REPORT, SAND2021-14614 (November 2021).

[5] Rozman, K.A., Saranam, V.R., Doğan, Ö. et al. “Effect of Specimen Orientation on the Mechanical Performance of Diffusion Bonded 316 Stainless Steel for Hybrid Printed Circuit Heat Exchangers.” J. of Materi Eng and Perform 30, 7950–7957 (2021). https://doi.org/10.1007/s11665-021-05980-1

[6] An, Z. L., Wang, W. X., Wang, Z. Y., & Tang, Y. F. “Performance of 316L Stainless Steel Diffusion Welding during High Temperature Creep.” Key Engineering Materials, 837, 22–27.

[7] Sah, Injin, Jong-Bae Hwang, and Eung-Seon Kim. 2021. "Creep Behavior of Diffusion-Welded Alloy 617" Metals 11, no. 5: 830. https://doi.org/10.3390/met11050830

[8] Mahajan, HP, Elbakhshwan, M, Beihoff, BC, & Hassan, T. "Mechanical and Microstructural Characterization of Diffusion Bonded 800H." Proceedings of the ASME 2020 Pressure Vessels & Piping Conference. Volume 3: Design and Analysis. Virtual, Online. August 3, 2020. V003T03A031. ASME. https://doi.org/10.1115/PVP2020-21502

[9] John Shingledecker, Vikash Kumar, Alex Bridges. “Observations in the High-Temperature Creep Performance of Diffusion Bonds for sCO2 Heat Exchangers.” Proceedings of ASME Turbo Expo 2023. ASME GT2023-102967 ©2023 ASME

[10] BPVC Section IX – Welding, Brazing, and Fusing Qualifications. BPVC-IX-2021, ASME (2021).

[11] “Case 2577.” BPVC Code Cases: Boilers and Pressure Vessels. BPVC-CC-BPV-2021, ASME (2021). ISBN: 9780791874325

[12] Shingledecker, J., Griscom, E. & Bridges, A. “Relationship between Grain Size and Sample Thickness on the Creep-Rupture Performance of Thin Metallic Sheets of INCONEL Alloy 740H.” *J. of Materi Eng and Perform* (2023). https://doi.org/10.1007/s11665-022-07785-2

[13] NIMS 316H LCF Data

[14] Youta Kashiwa, “Fatigue and Creep-Fatigue Acceptance Criteria for AM 316 Stainless Steel’ Thesis, Georgia Institute of Technology, August 2023.

[15] Kenji Kako, Eishi Kawakami, Joji Ohta, Masami Mayuzumi, Effects of Various Alloying Elements on Tensile Properties of High-Purity Fe-18Cr-(14-16)Ni Alloys at Room Temperature, MATERIALS TRANSACTIONS, 2002, Volume 43, Issue 2, Pages 155-162, Released on J-STAGE September 06, 2005, https://doi.org/10.2320/matertrans.43.155

[16] S.L. Mannan, K.G. Samuel, P. Rodriguez, “Influence of temperature and grain size on the tensile ductility of AISI 316 stainless steel,” *Materials Science and Engineering*, Volume 68, Issue 2, 1985, Pages 143-149, ISSN 0025-5416, https://doi.org/10.1016/0025-5416(85)90403-3

[17] S.L. Mannan, K.G. Samuel, P. Rodriguez, “The Influence of Grain Size on Elevated Temperature Deformation Behaviour of a Type 316 Stainless Steel,” Editor(s): R C GIFKINS, *Strength of Metals and Alloys (ICSMA 6),* Pergamon, 1982, Pages 637-642, ISBN 9781483284231, https://doi.org/10.1016/B978-1-4832-8423-1.50105-X.

[18] Swindeman, R.W., Sikka, V.K. & Klueh, R.L. “Residual and trace element effects on the high-temperature creep strength of austenitic stainless steels.” *Metall Mater Trans A* 14, 581–593 (1983). https://doi.org/10.1007/BF02643775

[19] Monteiro, Sergio Neves et al. “Creep Fracture Mechanisms and Maps in AISI Type 316 Austenitic Stainless Steels from Distinct Origins”. Materials Research [online]. 2017, v. 20, n. Suppl 2 https://doi.org/10.1590/1980-5373-MR-2017-0002

[20] M. Yamamoto, J. Shingledecker, C. Boehlert, T. Ogata, M. Santella. “Microscopic Evaluation of Creep-fatigue Interaction in a Nickel-based Superalloy.” *Proceedings: Creep & Fracture in High Temperature Components, 2nd ECCC Creep Conference*, April 21-23, 2009, Zurich, Switzerland.” © 2009 DEStech Publications, Inc. 1205-1215.

[21] Barua, Bipul, McMurtrey, Michael, Rupp, Ryann E., and Messner, Mark C. “Design Guidance for High Temperature Concentrating Solar Power Components.” United States: N. p., 2020. Web. doi:10.2172/1582656.

ACKNOWLEDGEMENTS

This work was funded by the U.S. Department of Energy’s Solar Energy Technology Office (National Lab Funding for Fiscal Years 2022, 2023, and 2024). Sandia National Laboratories is a multimission laboratory managed and operated by National Technology and Engineering Solutions of Sandia, LLC., a wholly owned subsidiary of Honeywell International, Inc., for the U.S. Department of Energy's National Nuclear Security Administration under contract DE-NA0003525.